UPDATE ON THE STATUS OF ODS ALLOYS FOR FOSSIL ENERGY APPLICATIONS

I.G. Wright and B.A. Pint

Oak Ridge National Laboratory, 1 Bethel Valley Road, MS 6156, Oak Ridge, TN 37831
E-mail: wrightig@ornl.gov; telephone: 865-574-4451; Fax: 865-241-0215

ABSTRACT

The goal of this project is to generate data that demonstrate and quantify earlier improvements in joining, microstructural modifications to minimize isotropy effects, and environmental lifetime modeling, in terms that can be readily assessed by potential users of oxide dispersion-strengthened (ODS) alloys. A report has been prepared compiling results from the literature of ODS alloy joining trials to provide a comprehensive documentation of the methods, procedures, and resulting microstructures and mechanical properties of joining methods available for use with ODS alloys. This report will be updated as continuing evaluations of joining techniques are completed and the results reported. Some further results from joining using pulsed plasma-assisted diffusion bonding, and transient liquid phase bonding are reported here. Long-term environmental exposures of representative ODS FeCrAl alloys in air have been completed, and data required for refinement of an oxidation-limited life-prediction model developed earlier are being generated from post-test analyses. Continuing exposures in a CO_2-steam mixture (at 1100°C in 500h cycles, with 1h at temperature each cycle and cooling to room temperature) have exceeded 3kh, and results so far indicate a greater degree of scale spallation than observed in air (in 100 h cycles), starting at 1 to 2kh for ODS alloys MA956 and PM2000, whereas much less scale spallation was observed for a non-ODS (weaker) model FeCrAlY alloy.

INTRODUCTION

Oxide dispersion-strengthened (ODS) alloys have significant advantages compared to all of the wrought, heat-resistant alloys that are available for consideration for application in the US Department of Energy's advanced systems for generating electricity or producing syngas or other fuels from coal. The ferritic ODS-FeCrAl alloys possess creep strength at temperatures significantly higher than are attainable with conventional alloys, as illustrated in Fig. 1 where extrapolated data for commercially-produced ODS alloys are compared to the best available data for the current classes of heat-resistant alloys [1].
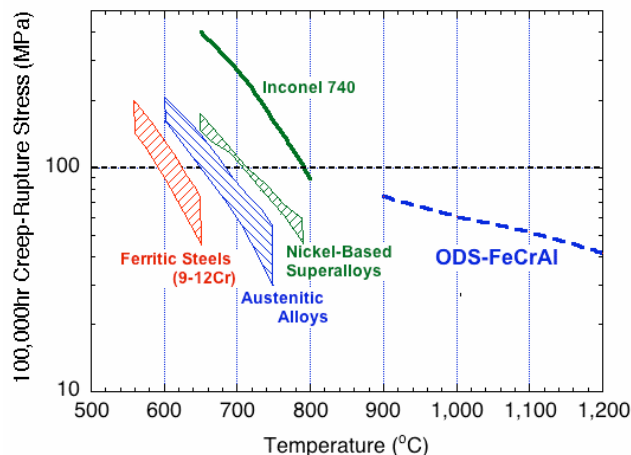

Figure 1. Comparison of the creep-rupture capabilities of the three major classes of heat-resistant alloys with an advanced, precipitation-strengthened, wrought Ni-based alloys (Inconel 740) and (extrapolated) data for ODS-FeCrAl alloys (after Shingledecker and Wright [1]).

This capability positions ODS alloys as an alternative choice for the lower end of the temperature range at which usually it is considered that ceramic materials must be used. A further advantage is the inherent resistance of ODS-FeCrAl alloys to high-temperature oxidation, which results from the formation of a slow-growing, external alumina scale, and exceptional resistance to oxide spallation.

These alloys have unusual properties as well as modes of behavior that are different from conventional, wrought, high-temperature alloys, so that there is a need to ensure that potential users of ODS alloys are aware of their peculiarities. ODS alloys are produced using a powder-metallurgical route involving high-energy milling, and so are expensive. There are also perceived problems with joining which have arisen because the standard fusion-welding approaches produce weak joints in these materials [2], since the particular microstructure needed to achieve creep strength is disrupted in the fusion zone. Further, in some product forms (particularly tubes) the alloy microstructure produced by typical processing routes results in highly-directional mechanical properties, which can lead to unusual mechanical behavior. In particular, high strain-rate sensitivity produces a relatively abrupt mode of failure. The efforts in this program are intended to address these issues, and to produce data to enable better-informed decisions to be made when process conditions are encountered where the properties of ODS alloys could be exploited.

RESULTS AND DISCUSSION

STRENGTH ANISOTROPY

The usual alloy microstructure developed in extruded tubes of ODS-FeCrAlY by secondary recrystallization typically has a very large length-to-diameter ratio, with the longest dimension in the axial direction. Such structures result in significant strength anisotropy, as illustrated by the lines drawn in Fig. 2 to represent the creep-rupture stress (as measured in 100h incrementally-loaded tests) in the axial and transverse directions for tubes of ODS-FeCrAl alloy PM2000 (see Table I for alloy compositions). In this project, the target that has been set for hoop strength for tube applications is to reproduce the type of alloy microstructure achieved in the Dour Metal Alloy ODM751 (Table I), shown in Fig. 3 (this alloy has not been available since the manufacturer went out of business in 1994). One of the approaches that has
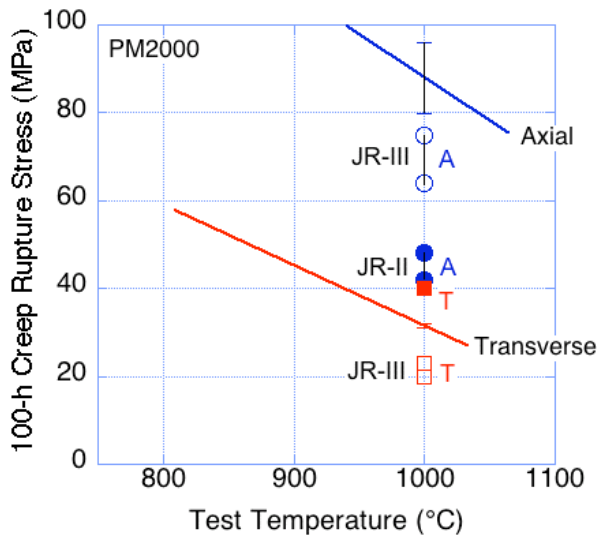

Figure 2. Creep-rupture results for tube samples of PM2000 as extruded and recrystallized recrystallized following controlled hot torsion
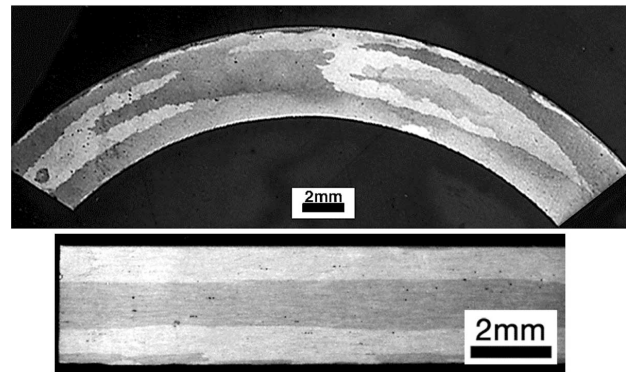

Figure 3. Cross sections of ODS-FeCrAl alloys ODM751 showing large, (solid lines), and "onion-skin" grain structure in the axial (top) and transverse (bottom) orientations

Table I. Compositions of Alloys of Interest (in atomic percent)

Alloy	Fe	Ni	Cr	Al	Mo	Ti	Si	Y	Zr	C	O^a	S^a	N^a
ODM 751	Bal	—	16.13	9.62	0.82	0.61	0.07	0.24	0	0.03	1.58	93	893
	Bal	—	16.36	7.57	0.85	0.65	0.11	0.24	0	0.03	1.62	82	918
MA956	Bal	—	20.05	8.77	0	0.40	0.13	0.24	0	0.06	0.65	41	608
	Bal	—	19.39	8.40	0	0.39	—	0.30	—	0.04	0.66	180	—
MA956HT	Bal	—	21.45	11.01	0.01	0.43	0.09	0.22	0	0.13	0.69	80	1059
	Bal	—	21.72	10.66	0.01	0.43	0.11	0.23	0	0.17	0.68	71	1064
PM2000	Bal	—	18.91	9.82	0.01	0.49	0.07	0.22	0	0.04	0.81	34	104
	Bal	—	20.02	10.62	0	0.44	0.04	0.23	0	0.03	0.74	50	211
ODS-Fe$_3$Al	Bal	—	2.13	27.07	—	0	0.05	0.21	0	0.16	0.62	30	3480
Kanthal APMT [b]	Bal	—	21.33	9.74	1.55	0.02	1.11	0.15	0.06	0.13	0.17	0	1512
	Bal	—	21.43	9.3	1.51	0.02	0.88	0.13	0.06	0.16	0.17	0	1979
FeCrAlY	Bal	—	20.59	10.22	—	—	—	0.04	—	0.009	0.007	—	253
Alloy 230 [c]	1.3	Bal	25.96	1.05	1.16	0.01	0.94	—	—	0.58	0.04	—	—
Inconel 693	4.7	Bal	29.99	6.23	0.02	0.47	0.10	—	0.03	0.123	—	—	401
Inconel 740 [d]	0.49	Bal	26.35	1.96	0.29	2.02	1.02	—	—	0.14	—	—	40

a: in ppma; b: +0.07Hf; c: +5.08 at% W; d: +1.21 at% Nb

been explored has been to try to influence the orientation of alloy grain growth during the secondary recrystallization step by imparting directional cold working into the alloy, in this case by using controlled torsional working to induce a spiral grain structure. Tubes of fine-grained (unrecrystallized) PM2000 were twisted to incrementally larger total torsional deformations and, after a secondary recrystallization heat treatment at 1380°C for 1 hr, specimens were removed (after flattening the tubes) to allow measurement of the effect of the modified grain structure on the creep behavior at 1000°C. Although the overall angle of twist of the tubes is known, the actual angle of the resulting grain structure to the direction of the creep loading in each specimen must be measured after creep testing to provide an accurate evaluation of the effectiveness of the microstructural manipulation. Preliminary creep results are shown in Fig 2, and indicate that for specimen JR-II (112.5° nominal torsion) the transverse creep strength was increased only slightly compared to the standard alloy, whereas the axial creep strength was significantly decreased. For specimen JR-III (119° nominal torsion), both axial and transverse creep strengths appeared to have been decreased. Without the benefit of post-test metallography (in progress), it is not possible to make meaningful correlations among angle of twist and creep behavior.

JOINING

While there are several processes available for joining ODS alloys [2], their applicability is highly dependent on the form of the alloy (tubing, rod, or sheet), and the intended final application of the component. Joining of ODS alloys must avoid redistributing the Y_2O_3 dispersed phase, and changing the size/shape/orientation of the alloy grain structure. As a result, processes that involve fusion tend to produce the weakest bonds due to disruption of dispersion and microstructure in the fusion zone, while processes where alloy grain growth can be induced to occur through the bond line are expected to produce the strongest joints [2]. The two joining processes studied in this project involve minimizing exposure to fusion.

(a) Transient Liquid-Phase (TLP) Bonding
This process involved the use of a 10 μm-thick foil of a low melting-point TLP alloy (produced by casting and rolling) between the parts to be joined, in this case 19 mm diam. rods of unrecrystallized PM2000. The ends of the rods in which the butt joints were to be made were machined flat and parallel with an as-machined mirror finish; the surfaces and TLP foil were degreased with alcohol and acetone before being joined in air. The rod samples and TLP foil were assembled in a compression platform fixture [3] and loaded at 5 MPa; the process steps consisted of heating to the bonding temperature (450°C) at 150-200°C/h, holding for 1 h to allow wetting and diffusion across the transient-liquid phase, followed by heating to a higher temperature (typically 900°C) and holding for a further 1 h to promote

diffusion of the components of the TLP phase away from the bond line. Post-bonding secondary recrystallization heat treatment (1h at 1380°C) was beyond the capabilities of the compression fixture, and so was conducted in a separate furnace. Despite several adjustments in the post-bonding heat treatment schedule, it was not possible to effect secondary recrystallization of the rods; recrystallized occurred only in a region up to 50 μm either side of the bond line to form larger (50-70 μm diameter), essentially equiaxed grains. In order to counter the apparent recovery of the pre-existing strain in the alloy by the post-bonding heat treatment, longitudinal slices were cut from the bonded rods and subjected to cold/warm rolling to reintroduce a level of cold work intended to drive subsequent secondary recrystallization. At the time of reporting, attempts to roll these specimens had failed, with the specimens breaking along the bond lines.

 (b) Pulsed Plasma-Assisted Diffusion (PPAD) Bonding

Creep testing at 1000°C was completed for a series of butt joints made by the PPAD bonding technique [4] using unrecrystallized (fine-grained) PM2000 that was subjected to the secondary recrystallization step either during the joining process or in a subsequent, separate heat treatment. The results for twenty-two tests are shown in Fig. 4; the specimens represented eleven variants of the processing conditions; eight tests were duplicates. Although the failure of some specimens was obviously associated with the presence of cracks or incomplete bonds, three specimens exhibited more than 81% of the <u>axial</u> failure load of the monolithic parent alloy, and a further four more than 62% of that load. The microstructures of specimens from the same rods after joining indicated that, in the cases that exhibited the highest loads to failure, not all of the typically five to six grains across the width of a given rod had fully grown through the bond line, suggesting that further improvements in processing may be possible. Nevertheless, a joint strength factor in excess of 81% is considered to be a most acceptable result.
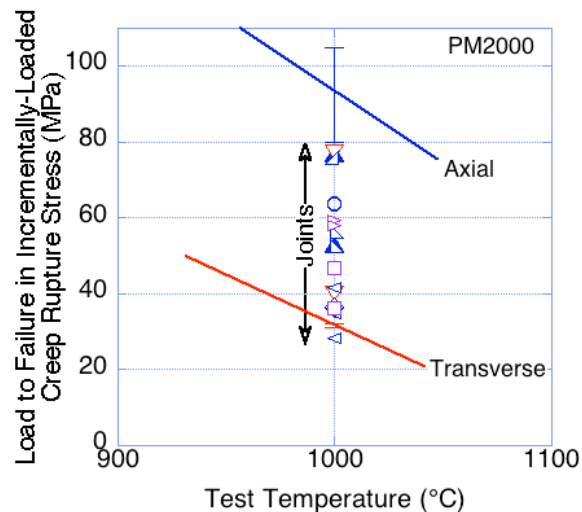

Figure 4. Creep strengths at 1000°C in air of butt joints made by PPAD bonding in fine-grained and subsequently recrystallized PM2000. The solid lines represent the creep strengths in the axial and transverse directions for the monolithic base alloy

OXIDATION-LIMITED SERVICE LIFETIME

ODS-FeCrAl alloys form continuous, external scales that are essentially pure α-Al$_2$O$_3$ and provide excellent protection in air to temperatures in excess of 1200°C. Because these scales are very slow growing and uniform in thickness, and there is negligible internal attack, the service life of the alloy cannot be equated to section thinning and measured in the usual way. However, the oxidation lifetime can be equated to the rate of Al consumption from the alloy to form the oxide scale [5,6], and this has formed the basis of an approach for modeling the oxidation kinetic behavior, hence for predicting oxidation-limited lifetimes [7]. Exposures of specimens to failure have been made to provide input for the model, and verification of its predictions. These exposures have involved multiple specimens exposed at 1000 to

1300°C in air for up to 30kh. Some exposures have been made in combustion environments (containing S, Cl), in air-water vapor mixtures, in steam, and recently in a CO_2-H_2O mixture intended to be an initial simulation of an oxy-firing environment.

(a) Oxidation in air

Figure 5a shows a compilation of the results of oxidation exposures run to failure for the five ODS-FeCrAl alloys listed in Table I, while runs still in progress are summarized in Fig. 5b. All exposures were made in 100 h increments (except at 1000°C, which involved 500h increments) with specimens cooled to room temperature and weighed after each increment. Individual specimens were exposed in lidded, alumina crucibles to allow measurement of the total oxygen uptake (total mass gain), and amount of scale lost due to spallation (weight of crucible+lid without specimen). The mass change of the specimen alone provided a basis for comparison with other tests in which crucibles typically are not (or cannot, in the case of mixed gases) be used. In Fig. 5, the units used for the abscissa are specimen volume (V)/specimen surface area (A); a tube of 25 mm OD x 2.5 mm wall has a V/A value of approximately 0.3, and that for a tube of 51 mm OD x 6 mm wall is 0.75; these values are indicated by vertical dashed lines in the figures. For considering the lifetime of components made from ODS sheet material, the service lifetime similarly could be expressed in terms of the thickness of the sheet.

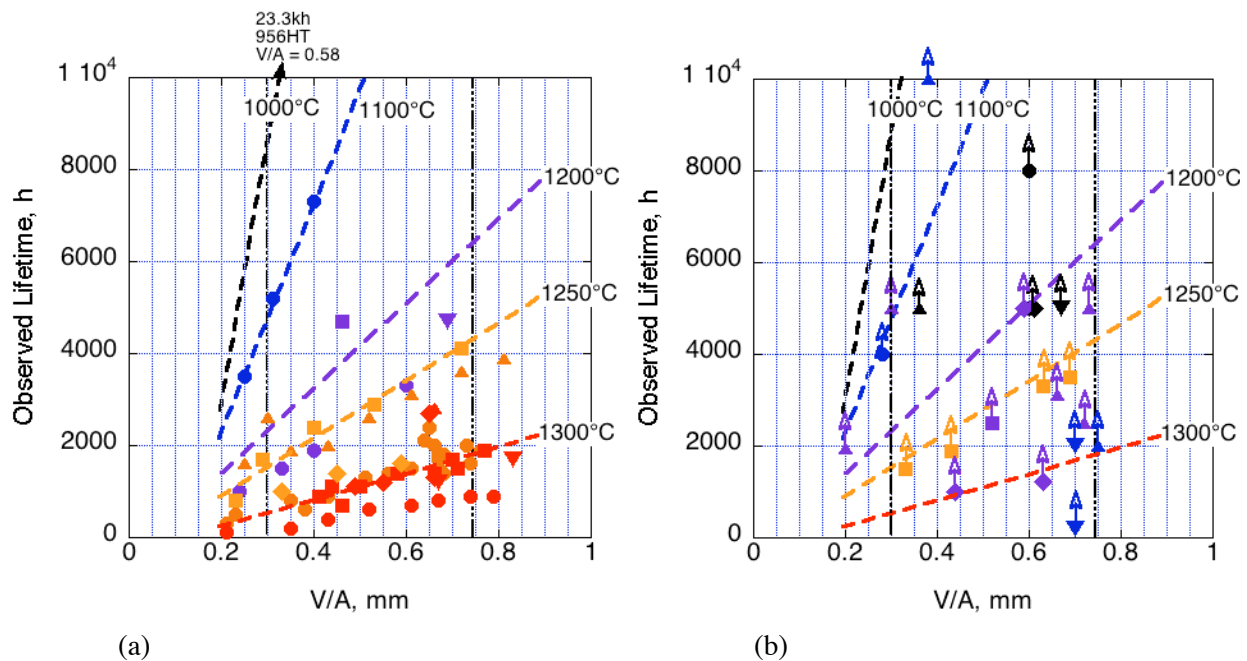(a)   (b)

Figure 5. Summary of cyclic oxidation exposures in air, run to failure at each of five temperatures, for MA956 (circles), MA956HT (squares), PM2000 (upright triangles), ODM751 (inverted triangles), and ODS-Fe_3Al (diamonds): (a) runs to failure; and (b) runs still in progress (color of symbols corresponds to the color assigned to each temperature).

The form of the oxidation life-prediction model has been discussed earlier [7]. The alloy oxidation kinetics are described as occupying three distinct stages: Stage 1 involves transient oxidation during which the equilibrium form of the scale is established; for the alumina scale-forming ODS alloys at the temperatures considered this stage is very short, and so mass gain/Al consumption in this stage was neglected. Stage 2 involves oxide growth according to a parabolic rate law, with negligible contribution from scale spallation, while in Stage 3 mass gain is considered to occur according to an overall linear rate law (contributions from oxide growth and loss by spallation). The scale thickness at which the transition from Stage 2 to Sage 3 occurs also is a required parameter. Thus, the effective service lifetime (t_b) can be simply expressed as: t_b = [length of the parabolic oxidation stage (Stage 2)] + [(Al remaining) / (rate of Al consumption during the linear oxidation stage in Stage 3)].

The algorithms derived from the kinetic data generated so far for describing the temperature-dependence of the Stage 2 and 3 rate constants, and the transition points, are listed in Table II.

Table II. Kinetic Terms Needed For Input For Oxidation-Limited Service Life Model

Alloy	Oxidation Kinetics Data		
	Kinetics, Stage 2	Kinetics, Stage 3	Transition, Stage 2-3
	k_2 g^{2}cm^{-4}s^{-1}	k_3 gcm^{-2}s^{-1}	μm
MA956	52.55 x e$^{-86,600/(1.987T)}$	0.607 x e$^{-57,350/(1.987T)}$	8.35x10^3 x e- $^{16,490/(1.987T)}$
MA956HT	7x10^{-4} x e$^{-55,261/(1.987T)}$	0.211 x e$^{-56,900/(1.987T)}$	73.8 x e$^{-2,940/(1.987T)}$
PM2000	1.01x10^{-2} x e$^{-64,463/(1.987T)}$	0.211 x e$^{-56,900/(1.987T)}$	2.17x10^4 x e$^{-20,560/(1.987T)}$
ODM751	0.18 x e$^{-72,727/(1.987T)}$	0.211 x e$^{-56,900/(1.987T)}$	2.17x10^4 x e$^{-20,560/(1.987T)}$
ODS-Fe$_3$Al	8.4 x e$^{-81,678/(1.987T)}$	221 x e$^{-75,908/(1.987T)}$	347 x e$^{-11,242/(1.987T)}$

Overall, the trends in oxidation behavior at each temperature were found to be very similar for all alloys, but MA956 typically exhibited the shortest lifetimes. The initial (parabolic) rate of oxidation of MA956 typically is faster than that of the similar MA956HT (by approximately 20% at 1200°C), which equates to a faster rate of Al consumption; the reason for this difference is not obvious from examination of the small differences in alloy compositions, especially the minor elements which might suggest a higher volume of carbides, for instance.

Post-test analysis of specimens has been used to extract not only oxidation kinetic data (rate of Al consumption), but also the minimum value of residual Al content at which protective behavior fails (to provide the total Al consumed usefully) [3]. An issue that has arisen is that some specimens removed from test at the point where end of life was assumed to be indicated by a sharp increase in the oxidation rate had, in fact, progressed sufficiently into breakaway oxidation that the alloy Cr content near the alloy-oxide interface was significantly depleted [3]. For those specimens the residual Al content was zero, and most likely not a true indication of the value required by the model. It is intended that the specimens shown in Fig. 5b as being 'tests in progress' be stopped short of breakaway oxidation (using scale color change to signify approach to breakaway) to provide the needed values of residual Al content. These analyses also indicated that the lifetimes measured for the typically rectangular specimens may underestimate those expected for tubes because of a tendency for localized scale spallation, hence waste of Al, at specimen corners. This issue was discussed earlier [8], but a satisfactory treatment has not yet been devised.

(b) Oxy-combustion-related CO_2-H_2O mixture
Exposures also have been made in a 50 vol% CO_2-50 vol% H_2O mixture at 1100°C and 1 atm. total pressure (calculated pO$_2$ = 3.8 x 10^{-5} atm.) to examine similarities and differences between a nominal flue gas composition representing oxy-firing conditions, and air (on which the lifetime model is based). Standard, parallelepiped specimens were exposed in non-enclosed alumina boats, oriented vertically so that the test gas flow was parallel to their major surfaces. The alloys exposed were: MA956, MA956HT, PM2000, ODS-Fe$_3$Al, a non-ODS FeCrAlY alloy used as a reference alumina-former, and three commercial alloys: IN693 (and alumina-former), Haynes 230, and Inconel 740, the latter two alloys representing the state-of-the-art in wrought high-temperature alloys (Table I). Four specimens of each alloy were exposed, and the tests were run in 500h segments, with cooling to room temperature and reweighing of the specimens after each segment. One specimen of each alloy was removed for destructive examination at 1kh intervals.

The mass change data derived from these exposures for ODS alloys MA956 and Fe$_3$Al are shown in Figs. 6a and b as data points (for all four replicates), and are compared to those in air at the same temperature (shown as lines). Both total mass gain and specimen mass change data are shown for exposures in air from tests involving 100 h thermal cycles. Since, for strong, alumina-forming alloys, little difference was
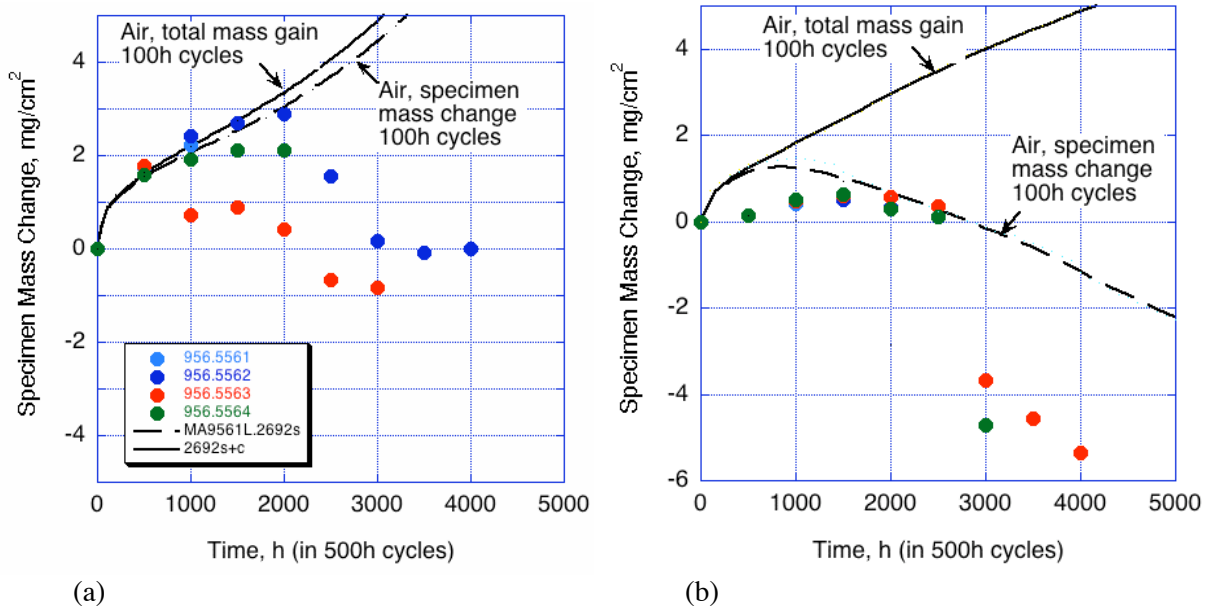
Figure 6. Comparison of mass change as a function of time at 1100°C in a 50% CO_2-50% H_2O mixture (500h cycles) and in air (100 h cycles) for (a) MA956; and (b) ODS-Fe_3Al.

found between scale spallation behavior for thermal cycling frequencies greater than 10h [9], it is expected that the specimen mass change curves from each of these test conditions should be directly comparable. The results in Fig. 6 indicate that the mass change in CO_2-H_2O of three of the four specimens of MA956, and all those of ODS-Fe_3Al followed those in air for up to 1kh and 2.5kh, respectively, after which both alloys exhibited a significantly greater amount of mass loss (scale spallation) than in air. Similar observations were made for alloys PM2000, non-ODS FeCrAlY, and Inconel 693.

Micrographs comparing the scale morphologies after 2kh in air and the CO_2-H_2O gas mixture for MA956, and Fig. 8 for ODS-Fe_3Al are shown in Fig. 7. While the overall appearance and thickness of the scales formed on MA956 were very similar in both gas mixtures, the scale formed in CO_2-H_2O exhibited numerous features along the alloy-oxide interface, as indicated by arrows 'A' in Fig. 7b, where the inward-growth of the oxide was irregular, as well as some areas where the scale had a lighter-colored appearance (arrow 'B') that were different from the small, light-colored inclusions typically present in such scales (as in Fig. 7a). Further, the alloy-oxide interface of the specimen exposed in CO_2-H_2O was noticeably more undulating than in air, a feature that often reflects relief of stress developed in the oxide layer.
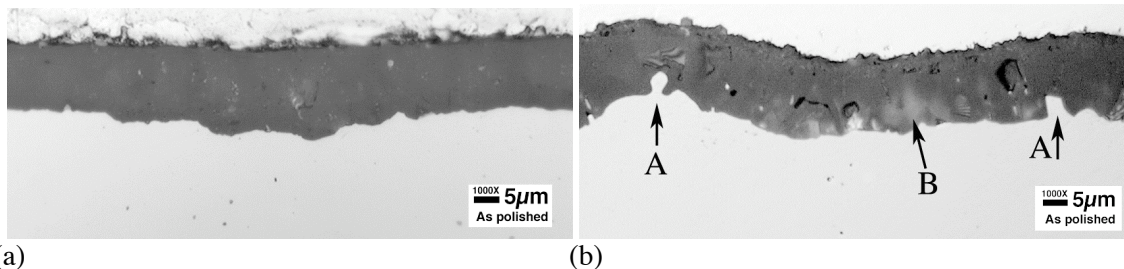

Figure 7. Cross sections of alloy MA956 after 2kh at 1100°C (a) in air, 100h cycles); and (b) in 50 vol% CO_2-50 vol% H_2O (500h cycles).

The thickness of the scale formed on ODS-Fe_3Al in CO_2-H_2O after 2kh was approximately twice that formed in air (Fig. 8). The fact that the specimen mass gains were very similar (Fig. 6b), is thought to reflect the fact that scale spallation was experienced from the start of the exposure in CO_2-H_2O, resulting in a less uniform overall scale thickness. A further major difference was the formation in CO_2-H_2O of a

semi-continuous outer layer of Fe-rich scale (identified by electron-probe microanalysis, and thought to be Fe_2O_3) that was not observed after exposure in air (the apparent outer layer on the air-formed oxide shown in Fig. 8a, and indicated by arrows, was an artifact from metallographic preparation of a specimen that was initially Cu-plated to preserve the friable oxide scale). There was no indication found of C enrichment in any part of the scale or alloy.
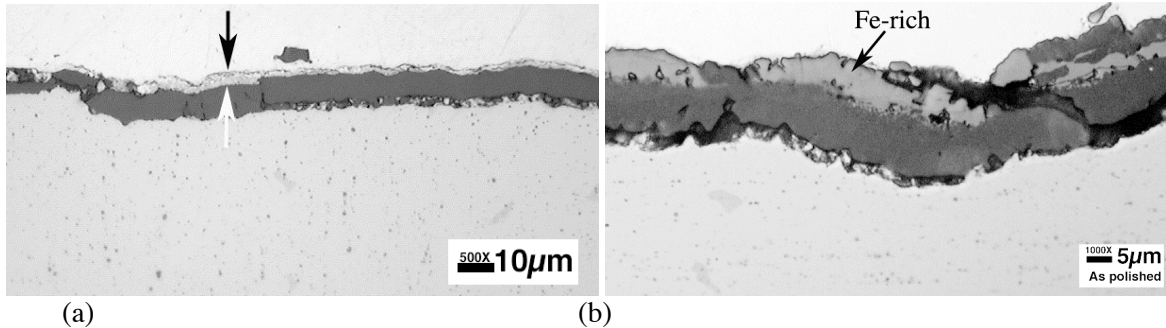

(a)   (b)

Figure 8. Cross sections of alloy ODS-Fe$_3$Al after 2kh at 1100°C (a) in air, 100h cycles); and (b) in 50 vol% CO_2-50 vol% H_2O (500h cycles).

Figure 9 indicates that the chromium oxide-forming Alloy 230 suffered significant and continuous mass loss in the CO_2-H_2O exposures; the data points represent the four individual specimens, and the line was drawn though the consolidated data set. Comparable kinetic data in air were not available. Similar mass loss behavior was observed for Inconel 740, although the rate of loss was much higher (155 vs. 7 mgcm^{-2} loss after 2kh). The micrographs in Fig. 10 indicate that the form of attack in Alloy 230 was very similar in air and the CO_2-H_2O gas mixture, with an external layer of Cr-rich oxide which also penetrated down alloy grain boundaries that intersected the surface, and the formation of discrete, fine particles of Al-rich oxide to a similar depth to that of the maximum grain boundary penetration. A major difference was that the depth of penetration of the internal attack appeared to be approximately 50% greater in the CO_2-H_2O gas mixture, reflecting either increased access of the gas to the alloy surface due to spallation of the external scale, or possibly increased oxygen transport through the external scale due to the presence of water vapor.
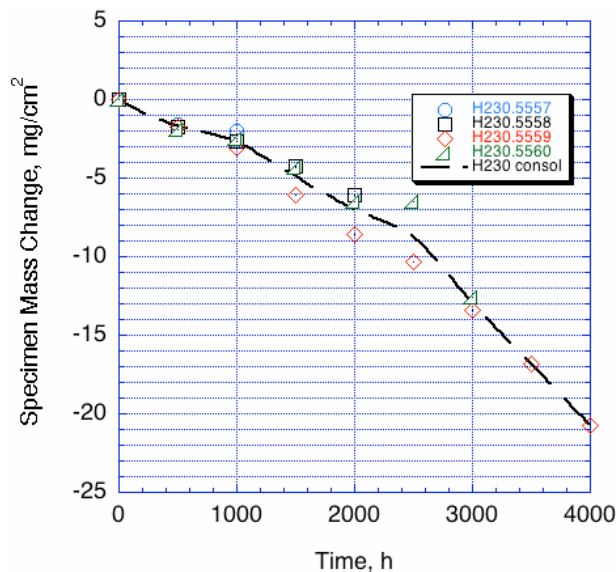

Figure 9. Mass loss for Alloy 230 at 1100°C in a 50% CO_2-50% H_2O mixture (500h cycles).

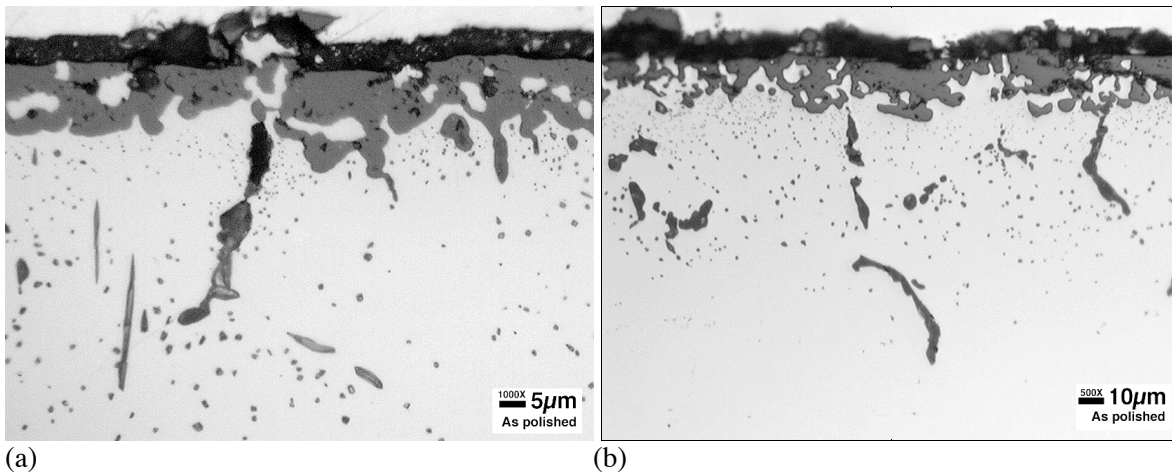(a)   (b)

Figure 10. Cross sections of Alloy 230 after 2kh at 1100°C (a) in air, 100h cycles); and (b) in 50 vol% CO_2-50 vol% H_2O (500h cycles).

SUMMARY

- While creep strength anisotropy in tubes made from alloys MA956 and PM2000 remains an issue, initial results from attempts to modify the aspect ratio of the recrystallized grain structure by controlled torsion of tubes after extrusion indicated that some changes can be effected in the axial and transverse creep strengths, but the extent that such modifications are useful remains to be determined from full analysis of the results.

- Completion of incremental creep testing of butt joints made in rods of PM2000 by pulsed plasma-assisted diffusion bonding confirmed that this technique can produce excellent joints with a most acceptable joint strength factor in excess of 81%, and that the range of processing conditions capable of such results is relatively wide.

- Most of the long-term oxidation exposures in air intended to determine actual oxidation-limited lifetimes have run for sufficient time to provide an acceptable basis for deriving the temperature-dependence of the oxidation kinetics, though not to fail many specimens at the lower temperatures (1100 and 1000°C). The parameters required by the model for lifetime prediction were derived and presented.

- Exposures in a 50 vol% CO_2-50 vol% H_2O gas mixture at 1100°C, intended to explore conditions expected in an oxy-firing scenario, indicated an increase in scale loss by spallation (compared to the behavior in air) for most of the alloys of interest. Initial characterization suggested some changes in scale morphology on MA956 and ODS-Fe_3Al that did not involve incorporation of C, but which may reflect some modification in the rate of developing the desired protective alumina scales.

ACKNOWLEDGMENTS

REFERENCES

1. J. P. Shingledecker and I. G. Wright, "Evaluation of the materials technology required for a 760ºC power steam boiler," pp. 107-119 in *Materials for Advanced Power Engineering 2006*, J. Lecomte-Beckers, M. Carton, F. Schubert, and P. J. Ennis, Eds., Schriften des Forschungszentrums Jülich (2006).
2. I.G. Wright, G.J. Tatlock, H. Al-Badairy, and C-L. Chen, *Summary of Prior Work on Joining of ODS Alloys*, Report on Task 8 of the UK-US Collaboration in Fossil Energy Advanced Materials Program, July 2008.
3. I.G. Wright, B.A. Pint, E.G. Dyadko, N.S. Bornstein, and G.J. Tatlock,"Enabling the practical application of oxide dispersion-strengthened ferritic steels," pp. in 78-94 in *Proc. 21ˢᵗ Ann. Conf. on Fossil Energy Materials,* R.R. Judkins and L.S. Mack, Eds., Oak Ridge National Laboratory Proceedings No. 008418, Dec. 2007.
4. E. Dyadko, "Novel Joining Technique for Oxide Dispersion-Strengthened Iron Aluminide Alloys," Quarterly report 7, under Contract No. DE-FG03-00ER83041, by Materials and Electrochemical Research (MER) Corporation, Tucson, AZ, September 30, 2003.
5. W. J. Quadakkers and K. Bongartz, *Werkstoffe und Korrosion*, 45, 232-41 (1994).
6. M.J. Bennett, H. Romary and J. B. Price, "The Oxidation Behavior of Alumina-Forming Oxide Dispersion-Strengthened Ferritic Alloys at 1200-1400°C," pp. 95-103 in *Heat Resistant Materials*, K. Natesan and D. J. Tillack, eds. (ASM, Materials Park, Ohio, 1991).
7. I.G. Wright, B.A. Pint, and Z.P. Lu, "Overview of ODS alloy development," *Proc. 19ᵗʰ Ann. Conf. on Fossil Energy Materials*, Marriott Hotel, Knoxville, Tennessee, May 9-11, 2005.
8. I.G. Wright, R. Peraldi, and B.A. Pint, "Influence of Aluminum Depletion Effects on the Calculation of the Oxidation Lifetimes of FeCrAl Alloys," *Material Science Forum*, 461-464, 579-589 (2004).
9. B.A. Pint, P.F. Tortorelli, and I.G. Wright, "Effect of cycle frequency on high-temperature oxidation behavior of alumina-forming alloys," *Oxidation of Metals*, 58 (1/2), 73-101 (2002).